arXiv:cond-mat/0205115v1 [cond-mat.str-el] 7 May 2002

Hole-doping dependence of percolative phase separation in $Pr_{0.5-\delta}Ca_{0.2+\delta}Sr_{0.3}MnO_3$ around half doping

D. Niebieskikwiat,* R.D. Sánchez, L. Morales, and B. Maiorov
Comisión Nacional de Energía Atómica-Centro Atómico Bariloche and Instituto Balseiro, 8400 Bariloche, Argentina
(March 22, 2022)

We address the problem of the percolative phase separation in polycrystalline samples of $Pr_{0.5-\delta}Ca_{0.2+\delta}Sr_{0.3}MnO_3$ for $-0.04 \leq \delta \leq 0.04$ (hole doping n between 0.46 and 0.54). We perform measurements of X-ray diffraction, dc magnetization, ESR, and electrical resistivity. These samples show at T_C a paramagnetic (PM) to ferromagnetic (FM) transition, however, we found that for $n > 0.50$ there is a coexistence of both of these phases below T_C. On lowering T below the charge-ordering (CO) temperature T_{CO} all the samples exhibit a coexistence between the FM metallic and CO (antiferromagnetic) phases. In the whole T range the FM phase fraction (X) decreases with increasing n. Furthermore, we show that only for $n \leq 0.50$ the metallic fraction is above the critical percolation threshold $X_C \simeq 15.5\%$. As a consequence, these samples show very different magnetoresistance properties. In addition, for $n \leq 0.50$ we observe a percolative metal-insulator transition at T_{MI}, and for $T_{MI} < T < T_{CO}$ the insulating-like behavior generated by the enlargement of X with increasing T is well described by the percolation law $\rho^{-1} = \sigma \sim (X - X_C)^t$, where t is a critical exponent. On the basis of the values obtained for this exponent we discuss different possible percolation mechanisms, and suggest that a more deep understanding of geometric and dimensionality effects is needed in phase separated manganites. We present a complete T vs n phase diagram showing the magnetic and electric properties of the studied compound around half doping.

I. INTRODUCTION

What is the origin of the "Colossal Magnetoresistance" (CMR)? Since the discovery of the CMR, an extensive research effort was done in this subject in order to elucidate the reasons for the appearance of an enormous reduction of the resistivity (ρ) with the application of a magnetic field (H) in the manganese perovskites $A_{1-x}A'_xMnO_3$ (A=La, Pr, Nd, Y and A′=Ca, Sr, Ba) and in other related half metals.[1–4] However, the complexity of the phase diagrams of these compounds indicate that the underlying mechanism of the CMR is not universal. In addition, the single- or poly-crystalline character of the samples also influences the magnetotransport response of the material. In strongly ferromagnetic (FM) compounds like $La_{2/3}Sr_{1/3}MnO_3$, the single crystals exhibit the CMR at the vicinity of the Curie temperature T_C as a linear decrease of ρ with H associated to the reduction of spin fluctuations, while polycrystals show a very different behavior, with a large fall of ρ at low fields (LFMR) followed by a much slower decrease of the resistance.[2] The LFMR is related to the reduction of the missalignment of the magnetization of contiguous grains and is enhanced with decreasing T. On the other hand, a much higher decrease of several orders of magnitude of ρ is achieved in charge-ordered antiferromagnetic (CO/AFM) compounds like $(Pr,Nd)_{1/2}Ca_{1/2}MnO_3$.[5,6] In this case the CMR is related to the transformation of the CO/AFM state into the FM metallic one, however magnetic fields of several tens of Teslas are necessary to observe this effect.

In the recent past, an interesting and potentially useful phenomenon of phase separation (PS) have been discovered.[7–19] The PS consists of the simultaneous coexistence of two or more magnetic (electronic) phases, like the FM, CO/AFM and paramagnetic (PM) ones. In phase separated manganites, the metal-insulator (MI) transitions occur in a percolative way, and a high CMR is achieved with moderated fields. With the application of a magnetic field an increase of the FM clusters is favored and the resistivity decreases due to the improvement of the geometrical factor for the current transport. Several workers have started to address the problem of percolation of the binary metal-insulator mixture, such as critical percolation thresholds and critical exponents, and its relation to CMR.[14–19] However, the wide range of possibilities given by the phase diagrams of low-bandwidth manganites makes these works just the beginning of the subject. For example, the major part of that previous research was done near doping 3/8, where CO appears at high T (but lower than T_{CO}) and the ground state is essentially FM metallic. On the other hand, in compounds presenting PS near half doping, as for example $Pr_{0.5}Ca_{0.2}Sr_{0.3}MnO_3$,[10] $Nd_{0.5}Sr_{0.5}MnO_3$,[12] and $La_{0.5}Ca_{0.5}MnO_3$,[13] the high temperature phase is the FM one (below T_C), and lowering T below T_{CO} it turns to a CO/AFM state.

The PS is observed in compounds which are located near first order MI transitions. In this sense, random disorder has been shown to play a fundamental role due to its ability to overcome the small energy dif-

ference between the competing phases near the transition, thus inducing the inhomogeneous state.[9,10] Transmission electron microscopy (TEM) studies at low T in $(La_{1-y}Pr_y)_{5/8}Ca_{3/8}MnO_3$ have shown that in the CO/AFM matrix there exist FM clusters of irregular shape with a size of several hundred of nanometers.[8] These observations make unlikely the charge segregation in this kind of phase separation, contrary to that observed in slightly doped AFM manganites.[20] The FM correlations inside a mainly CO/AFM phase is also observed in magnetization (M) measurements, which exhibit a clear FM component that allows to estimate the overall FM phase fraction X.[10]

The first order MI transition can be tuned, for example, by changing the average ionic radius of the A-site $\langle r_A \rangle$. This is the case of the $Pr_{0.65}Ca_{0.35-x}Sr_xMnO_3$ manganite,[11] which for $x = 0$ is CO/AFM and for $x = 0.35$ is FM metallic, while in the $x = 0.10$ composition the PS between these phases is observed. In the $(La_{0.25}Pr_{0.75})_{0.7}Ca_{0.3}MnO_3$ compound, Babushkina *et al.*[14] have explored the MI transition by partial oxygen isotope substitution.

In the present paper, we tune the MI transition by changing the hole concentration (n) in $Pr_{0.5-\delta}Ca_{0.2+\delta}Sr_{0.3}MnO_3$, where $n = 0.5 + \delta$, around half doping ($0.46 \leq n \leq 0.54$). Since the ionic radius of the Pr^{3+} and Ca^{2+} ions are similar, the advantage of this system is that $\langle r_A \rangle$ is kept constant, so the changes in the physical properties are intrinsically related to the variation of n. We show that almost the complete phase diagram of these samples is phase separated below T_C. In the whole temperature range the amount of FM phase continuously decreases with increasing n. In addition, the low temperature MI transition of the $n \leq 0.5$ samples is of percolative nature, i.e. for $T_{MI} < T < T_{CO}$ the resistivity decreases with increasing T due to the enlargement of X. In this T range the conductivity is successfully described in terms of the usual percolation theory, though possible geometrical and low-dimensional effects need to be considered. The CMR behavior for percolated samples is very different to that of the non-percolated ones.

II. EXPERIMENT

Powdered samples of $Pr_{0.5-\delta}Ca_{0.2+\delta}Sr_{0.3}MnO_3$ were prepared by the nitrate decomposition route. The raw materials (CO_3Sr, CO_3Ca and metallic Mn and Pr) were mixed in the stoichiometric amounts and disolved in nitric acid for the nitrates formation. Then the nitrates were heated at 800°C in air for 16h for their decomposition. The resulting powders were pressed into pellets and treated in air at 1450°C for 12h. Finally, the samples were cooled down to 800°C at 3°C/min and then quenched to room temperature.

The energy dispersive spectroscopy (EDS) experiments, carried out in a Philips 515 scanning electron microscope (SEM), indicate that the samples have no deviations from the nominal stoichiometry within the experimental resolution. The SEM observations also show well connected grains, whose sizes range from 3 to $6\mu m$. From thermogravimetric analysis (TGA) the oxygen content was found to be 3.000 ± 0.001.[21]

Powder X-ray diffraction (XRD) data were recorded on a Phillips PW 1700 diffractometer using CuKα radiation and a graphite monochromator. X-ray data at room temperature were refined by the Rietveld method with the FULLPROF program.[22]

The magnetization data as a function of T and H were measured between 10 and $300K$ in a commercial SQUID magnetometer equipped with a $5T$ magnet. Electron spin resonance (ESR) experiments were carried out in a Bruker ESP-300 spectrometer at 34GHz (Q-band) for $100K \leq T \leq 300K$. The electrical resistivity was measured by the usual four probe method in the $5 - 300K$ temperature range with $0 \leq H \leq 12T$.

III. RESULTS AND DISCUSSION

A. X-ray diffraction

The XRD results show that the samples mainly belong to the orthorhombic *Pbnm* space group. However, a minority amount of a tetragonal phase ($I4/mcm$ space group) is also present in the samples. In Fig. 1 we present the diffractogram of the sample $n = 0.54$, which has been satisfactorily adjusted proposing a model with both symmetries (the small vertical bars below the XRD data indicate the position of the Bragg reflections of both symmetries). From the Rietveld refinements, we found that the amount of tetragonal phase increases with increasing n, from 0% for $n = 0.46$ to $\sim 13\%$ at $n = 0.54$. In the inset of Fig. 1 we show a blow-up of the diffractograms of the $n = 0.46$, 0.50 and 0.54 samples, for 2θ between 46.25° and 48.25°. In this plot, a small peak can be clearly observed at $2\theta \approx 46.5°$ in the 0.54 sample, which gradually disappears with decreasing n. As labeled in the figure, this peak corresponds to the (004) reflection of the $I4/mcm$ symmetry. On the contrary, the intensity of the larger peak at $2\theta \approx 47.2°$ corresponding to the (220) reflection of the orthorhombic symmetry gradually increases with decreasing n. It can be also observed that the distortion of the majority orthorhombic phase is increased as n increases, as indicated by the larger splitting between the (220) and (004) reflections of the *Pbnm* space group.

Our XRD results are in agreement with the previous ones. The $Pr_{0.7}Sr_{0.3}MnO_3$ ($\delta = -0.2$ and $n = 0.30$ in our notation) has been found to belong to the orthorhombic *Pbnm* space group[23] while in the $Pr_{0.4}Ca_{0.3}Sr_{0.3}MnO_3$ compound ($\delta = 0.1$ and $n = 0.60$) the orthorhombic

phase was found to coexist with a small amount of the tetragonal one.[24]

B. Magnetization and ESR measurements

The magnetization as a function of T was measured at $H = 100Oe$ in zero-field cooling (ZFC) and field cooling (FC) processes, and is shown in Fig. 2 for all the samples studied. Although all the curves present similar transitions (PM to FM and then to AFM on lowering T), several differences are found. First at all, the M values clearly decrease a factor ~ 15 as n increases from 0.46 to 0.54. Second, qualitative differences can be observed between the samples in the left panels ($n \leq 0.50$) and those samples in the right ones ($n > 0.50$). For $n \leq 0.50$ the temperature where the ZFC and FC data collapse on a single curve remarkably coincides with the maximum of $|dM/dT|$, thus we identify that temperature as T_C. However, for $n > 0.50$ the T_C is much higher than the T where the maximum derivative occurs. In the following of the present section we will show that this behavior is related to the fact that the "FM" phase for the $n > 0.50$ samples is not a true long-range-order ferromagnet, but a coexistence with a majority PM phase is the true state. For these samples, the T of maximum derivative is an artifact generated by the growth of the FM phase fraction with decreasing T below T_C. Similarly, the low-T AFM state (at $T < T_{CO}$) is not a pure phase for all the samples, and it can be anticipated that the amount of FM component remains high in the $n = 0.46$ sample, while it decreases as n increases. An additional qualitative difference is observed for n below and above 0.5: for $n > 0.5$ a second increase of M is found for T below $T_h \sim 100K$, which we assume to be induced by the extra holes added into the insulating band of the CO $n = 0.50$ compound ($\delta = 0.02$ and 0.04 for $n = 0.52$ and 0.54, respectively).

The ESR spectra at 34GHz in Fig. 3 help us to distinguish the different magnetic contributions present in the samples. In this figure we present the results at four representative temperatures. In the spectra of the $n = 0.54$ composition there is superimposed the signal of a *dpph* marker, indicating the position of the spectroscopic splitting factor at $g = 2.00$.

Above T_C [see spectra in Fig. 3(d) at $270K$], all samples exhibit a resonance line corresponding to the PM mode, centered at $g \approx 1.97$ (independent of T) with a linewidth of $\sim 600Oe$. The temperature $207K$ corresponds approximately to the position of maximum magnetization for all the samples. At this T, what can be observed is that for $n = 0.52$ and 0.54 a second broad signal appears mounted over the still present PM line. On the contrary, in the $n \leq 0.50$ samples the PM resonance is almost not observed and the broad line appears alone. This second resonance is associated with a FM mode, and exhibits very different characteristics with respect to the PM one, namely, the center field is shifted to lower fields due to the appearance of an internal field, the linewidth is substantially larger, and the line presents an important asymmetry between the maximum and the minimum with respect to the base line. In all cases, the temperature where the FM behavior begins to manifest coincides with T_C (defined as the collapse of the ZFC and FC curves of Fig. 2). The different response for $n > 0.50$ indicates that below T_C these samples present a coexistence of the FM and PM phases. The onset of short-range FM order indicated by the splitting of the ZFC and FC data was also observed in the $Pr_{0.65}Ca_{0.35-x}Sr_xMnO_3$ compound.[11]

On lowering T below the CO temperature $T_{CO} \approx 175K$ (the temperature transition to the AFM state) the PM line is totally lost in all the samples. At $T = 150K$ the only observed response corresponds to the FM signal, which remains present also at $100K$. The presence of this signal indicates that below T_{CO} all the samples are phase separated, exhibiting the coexistence of the CO/AFM and FM phases.

In the spectra at $T = 100K$ it must be noted that the $n > 0.50$ samples present an additional line [labeled with an asterisk in Fig. 3(a)] at low fields $H \sim 2.5kOe$. The appearance of this resonance coincides with the increase of M below T_h. This resonance is likely not related to the FM phase, but it must occur within the CO volume. However, at this moment we cannot distinguish whether it is related to a homogeneous canting of the spins of the CO/AFM phase inducing a weak FM (WF) component or it corresponds to a third different (FM) phase. In spite of this, we note that WF modes in other materials have been found to appear at low fields.[25]

In order to quantify the amount of FM phase we measured $M(H)$ curves. The temperature dependent zero-field FM phase fraction $X(T)$ can be estimated from the T dependence of the spontaneous magnetization M_0 [the back-extrapolation of $M(H)$ to $H = 0T$]. To that end, we have measured for all the samples several $M(H)$ curves at different temperatures below T_C. We show these data in Fig. 4. To obtain these curves, the samples were previously heated up to the PM phase, then were cooled in zero field down to $10K$ and finally heated again to the measurement temperature. Therefore, the $X(T)$ data that we obtain from these measurements correspond to a ZFC and increasing T experiment.

The behavior observed in the $M(H)$ data of Fig. 4 even reinforce the features described above. It becomes clear in these curves that, although at $T_{CO} \approx 175K$ a FM to CO/AFM transition occurs, at $10K$ a FM component still persists. This FM component is another signature of the PS. It is also absolutely clear that at $10K$ none of the samples are totally FM since the saturated magnetization $M_S(n) = (4 - n)\mu_B$ is never reached.

The $n = 0.46$ sample, with the highest X exhibit FM-like curves. The sample with $n = 0.50$, below T_{CO} presents a pronounced hysteresis in the $M(H)$ curves. Initially these curves are also FM-like though they exhibit a low magnetization as compared with M_S, but

above a threshold field of the order of 1-2 Teslas M begins to increase rapidly. This behavior is due to the increase of the FM volume with increasing H. The increase of X with applied field is due to the gain of the Zeemann energy, which induces the swelling of the FM clusters. The need of a threshold field is probably related to the pinning of the interface between the FM and CO/AFM volumes. At $10K$, due to the hardness of the CO phase, fields much higher than $5T$ are needed to induce such a metamagnetic transition.[10]

The samples with $n > 0.50$ behave essentially similar at low T. However, for $T > T_{CO}$ these samples show, together with the small FM component, a predominant linear behavior at high fields. The slope is not other than the PM susceptibility that coexists with the short-range ferromagnetism. Indeed, when the temperature crosses T_C to the PM state this slope is preserved at similar values while the FM component disappears.

From the data in Fig. 4 we obtain the zero-field $X(T)$ as in previous works,[10] estimating from the Brillouin function the spontaneous magnetization $M_{0FM}(T)$ of a totally FM sample with the same M_S and T_C. After that,

$$X(t) = \frac{M_0(t)}{M_{0FM}(t)} \tag{1}$$

where $t = T/T_C$ is the normalized temperature. Despite of the mean-field approximation, this method correctly reproduces the T dependence of X.[10] The obtained results for the five samples are presented in Fig. 5. This figure somehow summarizes the conclusions of the magnetic measurements. In the whole T range X decreases with increasing n. This result is consistent with that expected from the XRD observations. Since the structural distortion decreases with decreasing doping, it is natural that the FM metallic phase is more favored at lower n. A similar doping evolution of X was observed by Huang *et al.*[13] in $La_{1-x}Ca_xMnO_3$ for x around 0.5. At $10K$ the X is $\approx 67\%$ for $n = 0.46$ and $\approx 4.6\%$ for $n = 0.54$ (a factor ~ 15, as in the M vs T curves of Fig. 2). At $n = 0.5$ we obtain $X \approx 18\%$, comparable to the 19% and 22% of $Nd_{0.5}Sr_{0.5}MnO_3$ and $La_{0.5}Ca_{0.5}MnO_3$, respectively.[12,13] For $n = 0.52$ and 0.54, if the increase of M for $T < T_h$ were generated by a homogeneous canting of the AFM phase, the obtained X at $T < T_h$ ($T/T_C < 0.4$) would be slightly higher than the actual value since the canting contribution would be included in the measured spontaneous magnetization.

At intermediate temperatures ($T/T_C \sim 0.7$), the CO/AFM to FM transition is seen as an important increase of X. At high T, the $n \leq 0.50$ samples are almost totally FM and X drops abruptly to zero at T_C, while the other two samples reach a maximum $X \sim 12\%$ at $T/T_C \sim 0.75$, after which the FM component smoothly vanishes as T approaches T_C. It is now clear that for $n > 0.50$, the variation of X above its maximum is responsible for the difference between T_C and the position of maximum derivative of the $M(T)$.

C. Percolative conductivity

In order to analyze the resistivity-FM fraction relation, we measured ρ vs T curves for all the samples at three different fields $H = 0$, 2, and $9T$, as shown in Fig. 6. Consequently with the X behavior, the resistivity increases with increasing n. Even more notable, the samples with $n \leq 0.5$ present a MI transition at T_{MI}, while the $n > 0.5$ samples show well insulating electrical properties with a resistivity several orders of magnitude higher. The abrupt change of ρ from $n = 0.50$ to 0.52 (more than four orders of magnitude at low T) is a clear indication that the metal-insulator transition between these samples has a percolative nature, as expected for disorder induced PS.[7] Also the MI transition as a function of temperature is of percolative type. As observed in Fig. 2, the samples with $n < 0.5$ do not exhibit any magnetic transition at T_{MI} justifying a metallic behavior below it. On the contrary, the abrupt fall of ρ above T_{MI} coincides with the T range where the magnetization begins to increase when the system approaches the AFM to FM transition at T_{CO} (the range $0.4 < T/T_C < 0.7$ in Fig. 5). Therefore, in this T range the resistivity response is unmistakable related to the changes of the FM phase fraction, i.e. at T_{MI} a percolative MI transition occurs. Between T_{MI} and T_{CO} the insulating-like response of ρ is given by the enlargement of the metallic paths with increasing T. Below T_{MI}, where the FM phase fraction is frozen, the resistivity of the $n \leq 0.5$ samples present metallic characteristics (slightly decreases with decreasing T) due to the intrinsic dependence of the metallic volume, and the residual ρ obviously decreases with increasing X. The fact that the samples with n above 0.5 are always insulating indicates that the percolation threshold is in between the X values of the 0.50 and 0.52 samples.

In order to understand the percolative behavior, in the range $T_{MI} < T < T_{CO}$ we obtained the conductivity ($\sigma = 1/\rho$) as a function of X for $n \leq 0.50$. In this temperature range, σ changes orders of magnitude due to the variation of X, thus the intrinsic T dependence of the metallic paths can be neglected, at least for $n = 0.50$ and 0.48. The resulting $\sigma(X)$ data are shown in Fig. 7 (the σ values were obtained from the $H = 0T$ warming curve, as in the X vs T experiment of Fig. 5). In the usual percolation theory, the σ vs X relation for X near above the percolation threshold (the so-called critical region) is given by[26]

$$\sigma \propto (X - X_C)^t \tag{2}$$

where X_C is the critical percolation threshold and t is the critical exponent. The way to obtain both these parameters is to construct a $\log\sigma$-$\log(X - X_C)$ plot, looking for the X_C which gives the best linear relation. Once X_C is obtained, the slope of this straight line is t. The proportionality factor in Eq. (2) is a sample dependent constant. In the inset of Fig. 7 we present the log-log

plot, where a quite fair linearity is observed and from which we obtained $X_C = 15.5(2)\%$ and $t = 0.96(5)$ (the σ of the $n = 0.50$ sample was multiplied by 2.45 in order to scale with the 0.48 data). The value of X_C is in very good agreement with three-dimensional (3D) percolation, where thresholds between 14 and 19% are expected.[26,27] This value of X_C also gives now a quantitative support to the expectation that the $n = 0.52$ and 0.54 samples are not percolated. The horizontal dotted line in Fig. 5 indicates the position of X_C, and it is very clear that both these samples have a X below the threshold in the whole temperature range. Therefore, the insulating state in these samples is an intrinsic behavior of the CO phase.

The almost linear relation between σ and X ($t = 0.96$) is somewhat surprising. In manganites the critical exponents are usually found to be between 2 and 4.[14–17] The implications of the value of t will be discussed below.

In order to study the percolation physics in the presence of a magnetic field, we have repeated the above analysis with an applied field $H = 2T$.

The magnetization of the $n = 0.48$ and 0.50 samples was measured by increasing T at $H = 2T$ after a FC process, since the $\rho(T)$ curves in Fig. 6 measured with nonzero field were obtained by this procedure. The $M(T)$ data are shown in Fig. 8, where all the magnetic transitions are still observed. In this case, the obtention of the FM phase fraction requires some considerations. On one hand, since the contribution of the AFM phase (M_{AFM}) at $H = 2T$ is different from zero, contrary to the case of the zero-field (spontaneous) magnetization M_0, the value of M is not directly proportional to X. Therefore, the M_{AFM} needs to be subtracted. On the other hand, when comparing with the magnetization of a totally FM sample, it must be done at the field $H = 2T$. However, this point can be neglected since for T below $0.75T_C$, in a totally FM material the difference between the magnetization at $H = 2T$ and the M_{0FM} is negligibly small. For example, in the $n = 0.46$ sample which at $T = 200K$ ($0.75T_C$) has a zero-field $X \approx 91\%$, the M_0 is $\approx 2.25\mu_B$ while the M at $H = 2T$ is $\approx 2.34\mu_B$, i.e. the difference is $\approx 4\%$, even including a minor contribution of the AFM volume and a possible field-induced increase of X. Finally, with the above considerations we can write

$$M \approx XM_{0FM} + (1 - X)M_{AFM} \quad (3)$$

The M_{AFM} can be obtained from the parent compound $Pr_{0.5}Ca_{0.5}MnO_3$, which is totally CO/AFM. Indeed, this compound exhibits well linear $M(H)$ curves with no spontaneous magnetization.[28] In the T range of our interest (75-175K), the susceptibility of this compound is weakly temperature dependent, lying between 0.040 and $0.045\mu_B/T$,[28] which indicates that $M_{AFM} \approx$ 0.08-0.09μ_B. After this contribution was taken into account, the X at $H = 2T$ was calculated from Eq. (3) and the σ vs X curve of Fig. 9 was obtained. In this case, to obtain the scaling with the $n = 0.48$ sample, the conductivity of the $n = 0.50$ one was multiplied by 1.8. The log-log plot of these data (inset of Fig. 9) also exhibits a good linear correlation with $X_C = 17.8(2)\%$ (also in agreement with 3D percolation), and the slope gives an exponent $t = 1.21(3)$, slightly higher than that without applied field. For comparison, in the same inset we have also included the straight line with slope $t = 0.96$ (dotted line) in order to highlight the increase of the exponent with the magnetic field.

D. Critical exponents: Relation to percolation mechanisms

Regarding the critical exponent, some experimental works have been performed in PS manganites. In some of them,[16] the authors used the exponent $t = 2$ expected for a mean-field behavior of the 3D percolation problem[29] and deduced X_C. In other cases,[14,15] as in this paper both X_C and t were deduced, and the obtained exponents lie in the range 2-4. However, these works were done at doping levels between 0.3 and 3/8, while our samples are situated around half doping. It is feasible that the precise percolation mechanism would depend on the doping level.

There are several ways to change the value of the critical exponent. A lot of experimental and theoretical work focused on this problem indicate that for 3D percolation, t lies between 1.5 and 2.[26,27,29,30] However, it has been shown that the conductivity exponent is nonuniversal,[31] and specific geometrical configurations of the contacts between percolating clusters could shift t to much higher values, e.g. by the formation of narrow necks. This is in agreement with the exponents found at the 0.3-3/8 doping range, but in our case t is well below 1.5.

There are other ways to produce a decrease on the critical exponent. One of them is also related to the geometry of the percolating clusters. It must be taken into account that the important parameter is not the conductivity, but the percolation probability $P(X)$ must be considered.[26] This probability represents the fraction of the sample which belongs to a percolated metallic path (thus $P(X) \leq X$). The percolation probability also has a critical behavior as in Eq. (2) with an exponent s which is typically ~ 0.5 for common lattice percolation models[26] and $s = 1$ for other sophisticated branching models which consider Bethe lattices.[32] Then, the conductivity can be obtained as[26,32]

$$\sigma(X) = \mu(X)P(X) \quad (4)$$

where μ is an effective mobility determined by the shape of the percolated (infinite) cluster. Therefore, the percolation probability $P(X)$ is an upper bound for the conductivity. The optimal case would occur if the connected region were arranged in regular arrays parallel to the applied electric field. This would result in the maximum μ, and the ratio of the conductivity of the whole material to the bulk conductivity of the metallic part would be equal

to $P(X)$,[26] then $t = s$. Indeed, the asymmetry observed in the FM signal in our ESR experiments could be showing some degree of shape anisotropy of the FM clusters. On the other hand, the intricate and constricted nature of the percolated paths reduce the mobility. For predominantly chain-like infinite clusters[32] $\mu \sim (X - X_C)$, thus $t \simeq s + 1$. As a conclusion, the role of the precise topology of the percolated clusters gives rise to a variety of nonuniversal exponents.

On the other hand, exponent values in the range 1-1.4 are naturally found in two-dimensional percolation systems.[26,30,33] This seems to contradict the fact that X_C remarkably coincides with the 3D threshold, however it must be taken into account that near half doping the mixed-valence manganites exhibit tendencies toward 2D metallic states in the AFM phase. For example $La_{1-x}Sr_xMnO_3$ for $x \gtrsim 1/2$, $Pr_{0.5}Sr_{0.5}MnO_3$, and $Nd_{0.45}Sr_{0.55}MnO_3$ all present the A-type AFM structure at low T.[34–37] In this magnetic phase the ab planes are ferromagnetically ordered, while contiguous layers have opposite spin direction. In the A-type phase, the electronic properties have been associated to a 2D metallic state due to a $d_{x^2-y^2}$ orbital ordering within the FM planes.[36–38] It is possible that in our $Pr_{0.5-\delta}Ca_{0.2+\delta}Sr_{0.3}MnO_3$ samples part of the AFM volume would be of the A-type, exactly in the same way as in $Nd_{0.5}Sr_{0.5}MnO_3$, where low T neutron powder diffraction (NPD) experiments show that 20% of the sample belongs to this phase.[12] Indeed, our samples share a common characteristic with the three previously mentioned A-type compounds. Those manganese perovskites present at room temperature a tetragonal crystal structure,[34–37] similar to the small amount of the $I4/mcm$ space group present in our samples. In fact, Woodward *et al.*[39] suggested that near half doping, this tetragonal space group favors the occupancy of the $d_{x^2-y^2}$ orbitals with the A-type AFM phase as ground state. The tetragonal volume in our samples should then produce the appearance of A-type AFM droplets at low T. Of course our magnetization measurements cannot distinguish between the CE-type (of the CO phase) and the A-type AFM states.

It could be possible that near the percolation threshold of the FM phase, some intercluster regions of the A-type connect the clusters as a sort of *valve* effect producing an effective 2D behavior, although the value of X_C determined by the dimensionality of the clusters themselves is unaltered. When a magnetic field is applied, the spins of the A-type AFM structure begin to orient in the field direction, with a consequent improvement of the electronic coupling between the otherwise decoupled metallic planes. This produces a field-induced dimensional crossover[37] from 2D to 3D that could be responsible for the increase of t from 0.96 to 1.21.

The above discussion makes totally clear the need of a close understanding of the percolation mechanism in phase-separated manganites. In this sense the geometry and effective dimensionality as well as doping evolution of the FM clusters become relevant.

E. Magnetoresistance

A notable feature in the $\rho(T)$ curves of Fig. 6 is that for $n \leq 0.50$ an appreciable CMR is obtained with a moderated field of $2T$, while for $n > 0.50$ at this field the resistivity remains almost unchanged. In the latter case, since the FM phase is not percolated the resistivity is dominated by the intrinsic behavior of the CO phase. A proof of this is given by Fig. 10, where we present MR vs H curves at $T = 50K$. For the percolated samples ($n \leq 0.50$), at the first stages of the ρ vs H loops ($H < 0.5T$) there is clearly visible a rapid decrease of ρ with increasing H, and after the field cycling (that produces a considerable hysteresis) the resistivity notably returns to its original value at $H = 0T$. The initial drop of ρ at low fields is related to the LFMR of polycrystalline FM manganites,[2] induced by the spin-polarized tunneling of electrons traveling through percolated paths that cross the grain boundaries. On the other hand, since the $n > 0.50$ samples are not percolated, there are no metallic paths connecting the electrodes across the whole sample. As a result, the rapid decrease of ρ at low fields is not observed. On the contrary, a smooth decrease occurs at low fields, typical of CO manganites. In addition, when the magnetic field is removed in the MR curves of Fig. 10(b), the resistivity does not go back to the initial value, but a much higher conductivity is retained. However, the insulating-like $\rho(T)$ curves in Figs. 6(d) and (e) indicate that, even in a FC process fields well above $9T$ are necessary to induce the percolation of the FM metallic phase in the $n > 0.50$ samples.

In order to show the field evolution of the X dependence of the MR, in Fig. 11 we show the zero-field $X(n)$ curve at $T = 50K$ in the top panel and in the bottom one the ratio $\rho(H)/\rho(0)$ vs n. It is clear that at low fields, the percolated samples exhibit the more important MR values. As the field increases above $1T$, however, the increase of the FM volume provides the dominant contribution producing better MR values in the $n = 0.50$ sample. As the field reaches much higher values, the relative change of resistivity shifts the higher MR values to the nonpercolated compounds (see the X_C line in the top panel).

The results shown in Fig. 11(b) indicate that the ideal materials to produce the highest MR values should be that located close to the percolation threshold. It would be even better if the zero-field FM phase fraction is located slightly below X_C, in such a way that a small applied field produces the increase of FM volume necessary to percolate the metallic phase thus raising the conductivity several orders of magnitude.[18,40]

F. Phase diagram

As a summary of our results, in Fig. 12 we present a complete zero-field T-n phase diagram. At high tem-

perature, the M and ESR measurements show that the samples are in the PM phase. On lowering T below T_C, FM correlations appear in all the samples. Although the T_C is symmetric around $n = 0.50$, in the samples with doping above this value the FM phase is not long-range-ordered, but coexists with a majority PM phase. In agreement with this, the $\rho(T)$ curves do not show any hint at T_C, while for $n < 0.5$ the resistivity presents a local maximum at that temperature.

At the CO temperature T_{CO} the samples turn into the CO/AFM state. However, a fraction of FM phase persists in all the samples down to the lowest temperatures. The region immediately below T_{CO} is characterized by insulating resistivities, however the electrical properties are again different depending on the doping level. For $n > 0.50$, due to the low values of X the insulating state is given by an intrinsic response of the CO volume. On the contrary, for $n \leq 0.50$ the decrease of the FM volume fraction with decreasing T promotes the insulating behavior, though there are percolated metallic paths. In these samples, when the FM phase fraction is frozen a MI transition occurs at T_{MI}, below which the T evolution of ρ is intrinsic of the metallic phase. Between T_{MI} and T_{CO} is where the usual percolation theory accounts for the conductivity variation.

The temperature T_h for $n > 0.50$ indicates the additional magnetization increase at low T with the simultaneous appearance of a low-field resonance line in the ESR spectra. Although this is labeled in the phase diagram as the F' phase, at this moment we cannot distinguish whether this contribution comes from a third phase or from a homogeneous canting of the AFM state. NPD experiments are being performed to elucidate the origin of this magnetic component. These experiments will also help to probe whether or not there exists a small A-type AFM volume in the samples studied here.

By extrapolating the FM fraction toward lower holes concentration, we estimate that for $n \sim 0.43$ the material should be 100% FM. At this doping level the T_{MI} and T_{CO} should collapse at the same value, and the compound should present metallic properties in the whole T range below T_C. The $Pr_{0.6}Ca_{0.1}Sr_{0.3}MnO_3$ ($n = 0.40$) and the limiting compound $Pr_{0.7}Sr_{0.3}MnO_3$ ($n = 0.30$) are indeed in this situation.[41] For $n > 0.50$ the FM phase is strongly suppressed and the material is essentially CO, in agreement with the much higher structural distortion. In the intermediate region, where the first order phase transition occurs between the metallic and insulating phases the PS is observed, where X smoothly decreases with increasing n producing a percolative MI transition.

IV. SUMMARY

We studied the magnetic and electric properties of polycrystalline $Pr_{0.5-\delta}Ca_{0.2+\delta}Sr_{0.3}MnO_3$ around half doping. The magnetization and ESR measurements allowed us to characterize the magnetic states of the compound in the whole T range, as well as to obtain the FM phase fraction X of the PS states as a function of temperature. Consequently with the FM phase fraction behavior, the electrical properties are distinguishable different for n below and above 0.50, related to the percolative metal-insulator transition as a function of doping. In the percolated samples ($n \leq 0.50$), the increase of resistivity with decreasing T below T_{CO} is related to the reduction of the FM volume. In this T range, the conductivity follows the percolative behavior $\sigma \sim (X - X_C)^t$. The values obtained for X_C are in agreement with that expected for conventional 3D percolation. However, the low values obtained for t depart from that observed in other compounds, indicating that there should be different percolation mechanisms. On one hand the geometric configuration of the FM clusters is an important issue that needs to be addressed, and on the other hand possible 2D effects could also produce this behavior. In this sense, the increase of t with applied field could indicate a field-induced dimensional crossover.

With respect to the MR response, we showed that FM fractions near X_C are the optimal for producing large MR ratios with moderated fields. In fact, the percolated samples show very different magnetoresistance properties, specially at low fields.

Finally, the presented T-n phase diagram shows that in a small region of doping level around 1/2 several electronic phases need to be considered. The asymmetric electronic properties observed around half doping can be regarded as related to the doping dependence of the FM phase fraction, i.e. at half doping the percolation of the FM metallic phase occurs.

ACKNOWLEDGMENTS

We thank A. Caneiro, A.A. Aligia, and J. Milano for useful discussions and for the critical reading of this manuscript. This work was supported by CNEA (Comisión Nacional de Energía Atómica), CONICET (Consejo Nacional de Investigaciones Científicas y Técnicas), Fundación Antorchas and ANPCyT (Agencia Nacional de Promoción Científica y Tecnológica, Argentina), PICT 99-03-05266. RDS and LM acknowledge the CONICET for financial support.

* Author to whom correspondence should be addressed. E-mail address: niebied@cab.cnea.gov.ar

[1] S. Jin, T.H. Tiefel, M. McCormack, R.A. Fastnach, R. Ramesh, and L.H. Chen, Science **264**, 413 (1994).

[2] H.Y. Hwang, S-W. Cheong, N.P. Ong, and B. Batlogg, Phys. Rev. Lett **77**, 2041 (1996).

[3] J.M.D. Coey, A.E. Berkowitz, Ll. Balcells, F.F. Putris, and A. Barry, Phys. Rev. Lett. **80**, 3815 (1998).
[4] D. Niebieskikwiat, A. Caneiro, R.D. Sánchez, and J. Fontcuberta, Phys. Rev. B **64**, 180406(R) (2001); K.-I. Kobayashi, T. Kimura, H. Sawada, K. Terakura, and Y. Tokura, Nature (London) **395**, 677 (1998).
[5] Y. Tokura and Y. Tomioka, J. Magn. Magn. Mater. **200**, 1 (1999), and references therein.
[6] M. Tokunaga, N. Miura, Y. Tomioka, and Y. Tokura, Phys. Rev. B **57**, 5259 (1998); M. Respaud, A. Llobet, C. Frontera, C. Ritter, J.M. Broto, H. Rakoto, M. Goiran, and J.L. García-Muñoz, *ibid* **61**, 9014 (2000).
[7] E. Dagotto, T. Hotta, and A. Moreo, Phys. Rep. **344**, 1 (2001); A. Moreo, S. Yunoki, and E. Dagotto, Science **283**, 2034 (1999).
[8] M. Uehara, S. Mori, C.H. Chen, and S-W. Cheong, Nature (London) **399**, 560 (1999).
[9] A. Moreo, M. Mayr, A. Feiguin, S. Yunoki, and E. Dagotto, Phys. Rev. Lett. **84**, 5568 (2000).
[10] D. Niebieskikwiat, R.D. Sánchez, A. Caneiro, and B. Alascio, Phys. Rev. B **63**, 212402 (2001).
[11] D. Niebieskikwiat, R.D. Sánchez, and A. Caneiro, J. Magn. Magn. Mater. **237**, 241 (2001).
[12] C. Ritter, R. Mahendiran, M.R. Ibarra, L. Morellon, A. Maignan, B. Raveau, and C.N.R. Rao, Phys. Rev. B **61**, R9229 (2000).
[13] Q. Huang, J.W. Lynn, R.W. Erwin, A. Santoro, D.C. Dender, V.N. Smolyaninova, K. Ghosh, and R.L. Greene, Phys. Rev. B **61**, 8895 (2000).
[14] N.A. Babushkina, A.N. Taldenkov, L.M. Belova, E.A. Chistotina, O. Yu. Gorbenko, A.R. Kaul, K.I. Kugel, and D.I. Khomskii, Phys. Rev. B **62**, R6081 (2000).
[15] V. Hardy, A. Wahl, and C. Martin, Phys. Rev. B **64**, 064402 (2001).
[16] K.H. Kim, M. Uehara, C. Hess, P.A. Sharma, and S-W. Cheong, Phys. Rev. Lett. **84**, 2961 (2000).
[17] V. Podzorov, M. Uehara, M.E. Gershenson, T.Y. Koo, and S-W. Cheong, Phys. Rev. B **61**, R3784 (2000).
[18] M. Mayr, A. Moreo, J.A. Vergés, J. Arispe, A. Feiguin, and E. Dagotto, Phys. Rev. Lett. **86**, 135 (2001).
[19] Y. Xiong, S-Q. Shen, and X.C. Xie, Phys. Rev. B **63**, 140418(R) (2001).
[20] G. Allodi, R. De Renzi, G. Guidi, F. Licci, and M.W. Pieper, Phys. Rev. B **56**, 6036 (1997); M. Hennion, F. Moussa, G. Biotteau, J. Rodríguez-Carvajal, L. Pinsard, and A. Revcolevschi, Phys. Rev. Lett. **81**, 1957 (1998).
[21] D. Niebieskikwiat *et al.*, to be published.
[22] Fullprof program, J. Rodríguez-Carvajal, Laboratoire Léon Brillouin (CEA-CNRS), v/October 1998.
[23] K. Knížek, Z. Jirák, E. Pollert, F. Zounova, and S. Vratislav, J. Sol. State Chem. **100**, 292 (1992).
[24] A. Barnabé, M. Hervieu, C. Martin, A. Maignan, and B. Raveau, J. Phys. Chem. Solids **62**, 1365 (2001).
[25] A. Fainstein, A. Butera, R.D. Zysler, M. Tovar, C. Rettori, D. Rao, S.B. Oseroff, Z. Fisk, S-W. Cheong, D.C. Vier, and S. Schultz, Phys. Rev. B **48**, 16775 (1993); A. Fainstein, A. Butera, and M. Tovar, *ibid* **50**, 16708 (1994).
[26] S. Kirkpatrick, Rev. Mod. Phys. **45**, 574 (1973), and references therein.
[27] I. Webman, J. Jortner, and M.H. Cohen, Phys. Rev. B **14**, 4737 (1976); H. Scher and R. Zallen, J. Chem. Phys. **53**, 3759 (1970).
[28] S. Krupička, M. Maryško, Z. Jirák, and J. Hejtmánek, J. Magn. Magn. Mater. **206**, 45 (1999).
[29] S. Kirkpatrick, Phys. Rev. Lett. **36**, 69 (1976).
[30] T.J. Coutts, Thin Solid Films **38**, 313 (1976), and references therein.
[31] S-I. Lee, Y. Song, T.W. Noh, X-D. Chen, and J.R. Gaines, Phys. Rev. B **34**, 6719 (1986); B.I. Halperin, S. Feng, and P.N. Sen, Phys. Rev. Lett. **54**, 2391 (1985); P.M. Kogut and J.P. Straley, J. Phys. C **12**, 2151 (1979).
[32] R.B. Stinchcombe, J. Phys. C **6**, L1 (1973); *ibid* **7**, 179 (1974).
[33] M.A. Dubson and J.C. Garland, Phys. Rev. B **32**, 7621 (1985).
[34] Z. Jirák, J. Hejtmánek, K. Knížek, M. Maryško, V. Šíma, and R. Sonntag, J. Magn. Magn. Mater. **217**, 113 (2000).
[35] T. Akimoto, Y. Maruyama, Y. Moritomo, A. Nakamura, K. Hirota, K. Ohoyama, and M. Ohashi, Phys. Rev. B **57**, R5594 (1998); Y. Moritomo, T. Akimoto, A. Nakamura, K. Ohoyama, and M. Ohashi, *ibid* **58**, 5544 (1998); J. Dho, E.O. Chi, W.S. Kim, N.H. Hur, and Y.N. Choi, *ibid* **65**, 132414 (2002).
[36] D. Niebieskikwiat and R.D. Sánchez, J. Magn. Magn. Mater. **221**, 285 (2000).
[37] H. Kuwahara, T. Okuda, Y. Tomioka, A. Asamitsu, and Y. Tokura, Phys. Rev. Lett. **82**, 4316 (1999).
[38] R. Maezono, S. Ishihara, and N. Nagaosa, Phys. Rev. B **57**, R13993 (1998); *ibid* **58**, 11583 (1998); J.H. Jung, H.J. Lee, J. Yu, and T.W. Noh, Phys. Rev. B **61**, 14656 (2000).
[39] P.M. Woodward, T. Vogt, D.E. Cox, A. Arulraj, C.N.R. Rao, P. Karen, and A.K. Cheetham, Chem. Mater. **10**, 3652 (1998).
[40] N.A. Babushkina, L.M. Belova, D.I. Khomskii, K.I. Kugel, O. Yu. Gorbenko, and A.R. Kaul, Phys. Rev. B **59**, 6994 (1999).
[41] J.G. Lin, J. Phys. Chem. Solids **62**, 1881 (2001).

FIG. 1. Room temperature X-ray diffractogram of the sample with doping $n = 0.54$. ($\circ$) Experimental data and (—) Rietveld refinement using a model with two symmetries: the orthorhombic $Pbnm$ and the tetragonal $I4/mcm$. (|) Bragg reflections of both these symmetries. The lower solid line centered at -0.25 is the difference between the experimental data and the refinement. Inset: Blow-up of a selected region of the diffractograms of the indicated samples. This shows the increase of the amount of tetragonal phase with increasing n.

FIG. 2. Magnetization vs temperature at $H = 100Oe$ in ZFC (lower curves) and FC (upper curves) processes. The doping level is indicated in each case. The T_C is the temperature where the ZFC and FC data collapse on a single curve.

FIG. 3. ESR spectra obtained at $34GHz$ for all the samples (as labeled) at four representative temperatures indicated in the panels. The narrow line mounted over the spectra for $n = 0.54$ corresponds to the *dpph* marker,

which indicates the value $g = 2.00$. The asterisks in panel (a) show the additional line that appears at the temperature $T_h \sim 100K$.

FIG. 4. $M(H)$ curves at several T for the four samples indicated. The sample with $n = 0.48$ (not shown) presents an intermediate behavior between $n = 0.46$ and 0.50. All these curves were obtained after heating the samples up to the PM phase, followed by a ZFC to $10K$ and subsequent heating to the T of the measurement.

FIG. 5. Zero-field FM phase fraction X as a function of the reduced temperature. The samples with $n > 0.50$ show a small FM volume which does not percolate, while for $n \leq 0.50$ the high X values lie above the percolation threshold X_C (dotted line).

FIG. 6. T dependence of the resistivity for all the samples at several applied fields. Those curves measured with $H \neq 0T$ were obtained in FC process. The arrows indicate the direction of the temperature variation and T_{MI} the metal-insulator transition temperature for the $n \leq 0.50$ samples.

FIG. 7. Conductivity vs FM phase fraction (X). The data of the $n = 0.50$ sample were multiplied by 2.45. The line is a fit with the percolation law $\sigma \sim (X - X_C)^t$ Inset: σ vs $(X - X_C)$ in log-log scales, showing the percolative behavior with the indicated values of X_C and the exponent t.

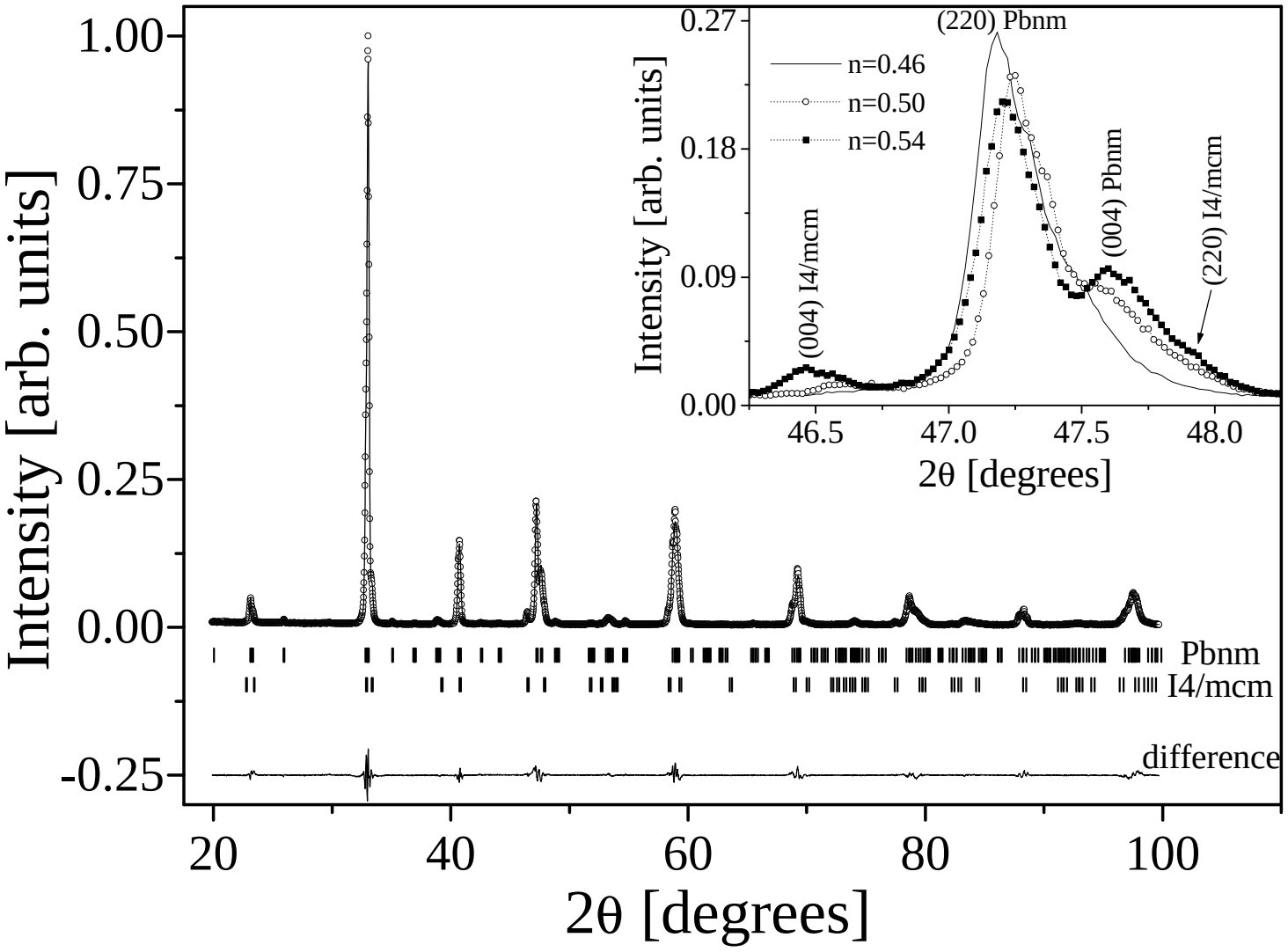
FIG. 8. M vs T for $n = 0.48$ and 0.50 measured with an applied field $H = 2T$ and increasing temperature after a FC process.

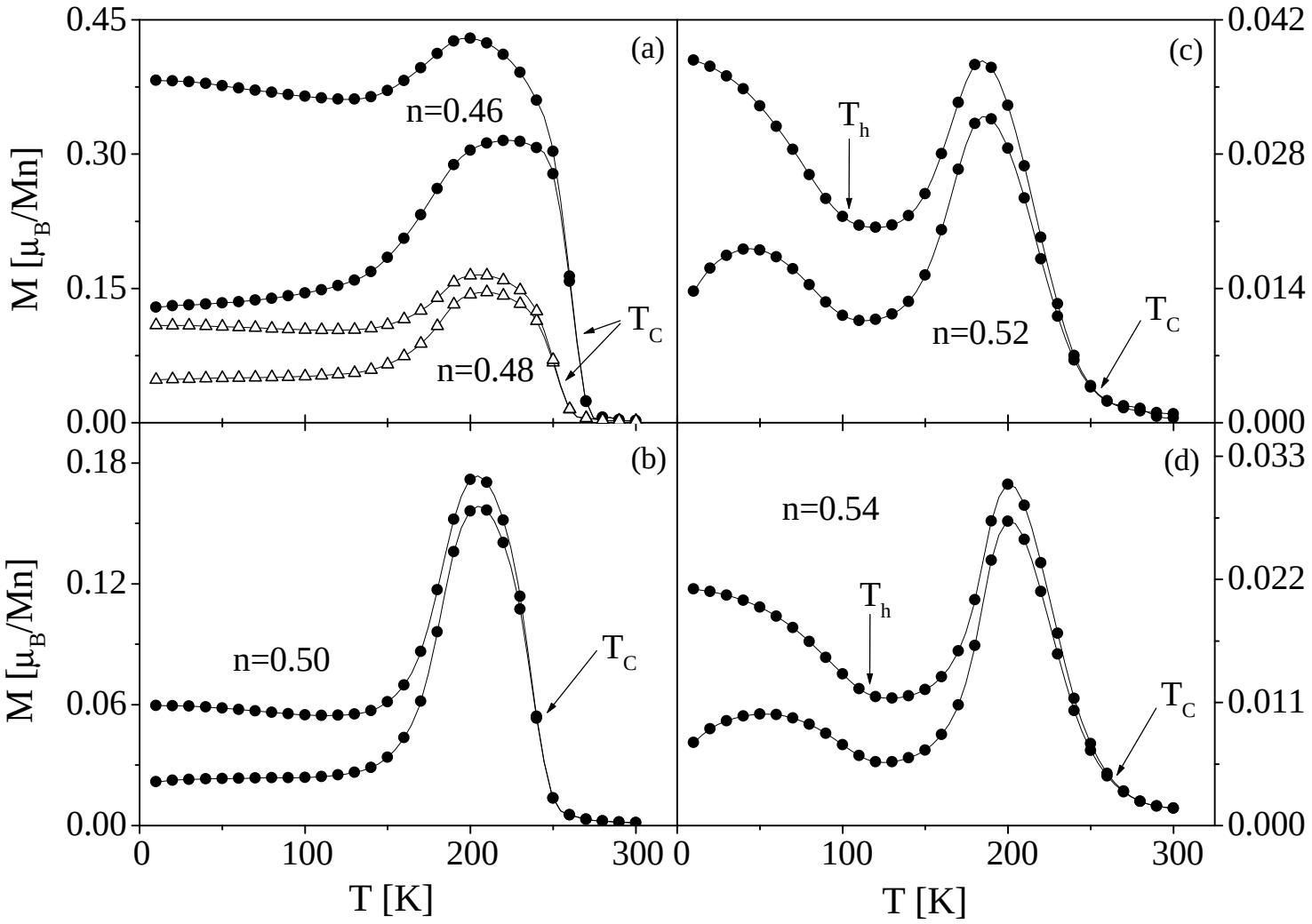
FIG. 9. X dependence of σ at $H = 2T$. In this case the σ for $n = 0.50$ was multiplied by 1.8. The data are well fitted with Eq. (2) using $X_C = 17.8\%$ and $t = 1.21$ (solid line). Inset: $\log \sigma$ vs $\log(X - X_C)$, where a linear dependence characteristic of a percolation process is observed. The straight dotted line corresponds to an exponent $t = 0.96$, obtained at zero-field.

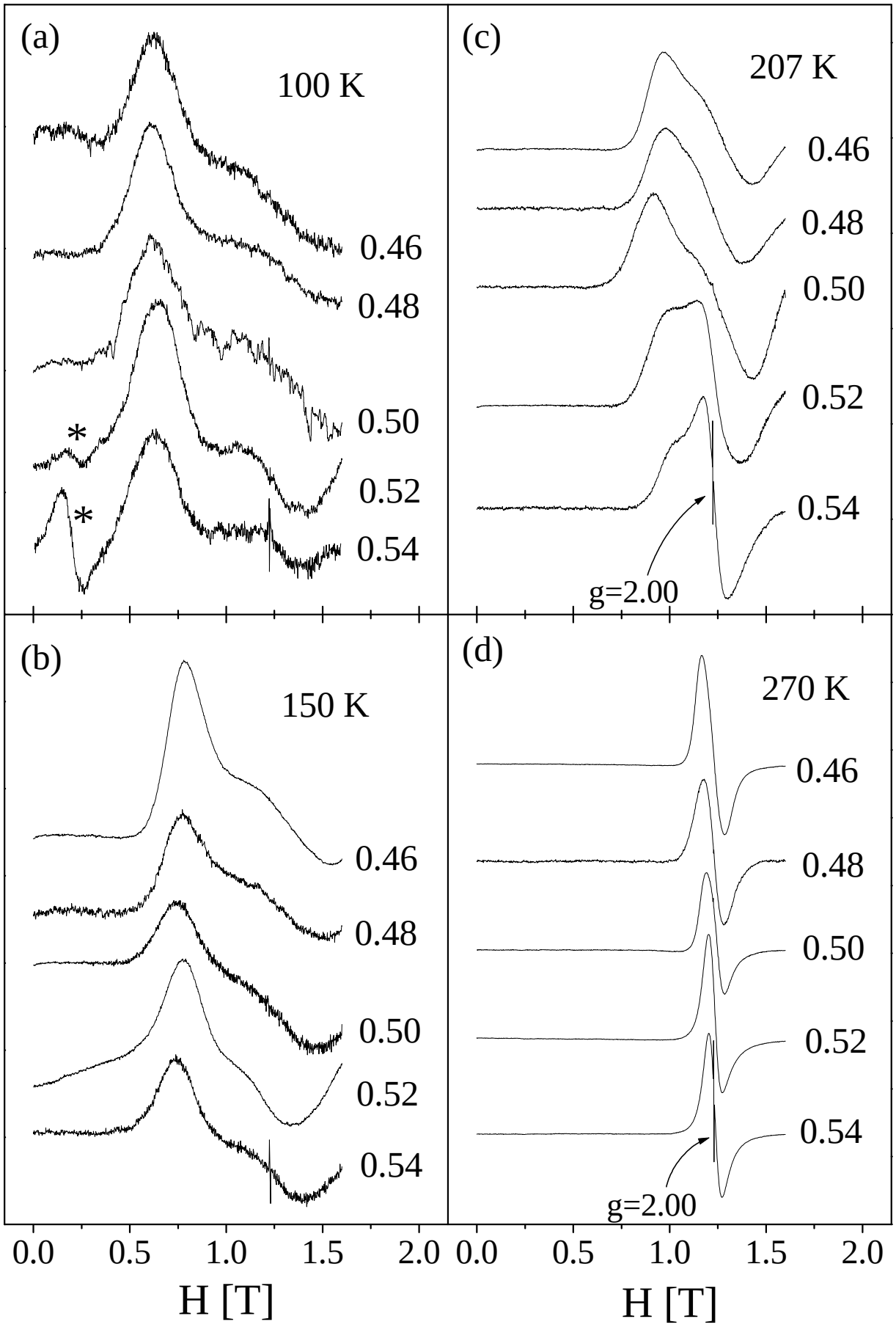
FIG. 10. Magnetoresistance vs H at $T = 50K$ of all the studied samples, as labeled. The arrows indicate the direction of the field variation.

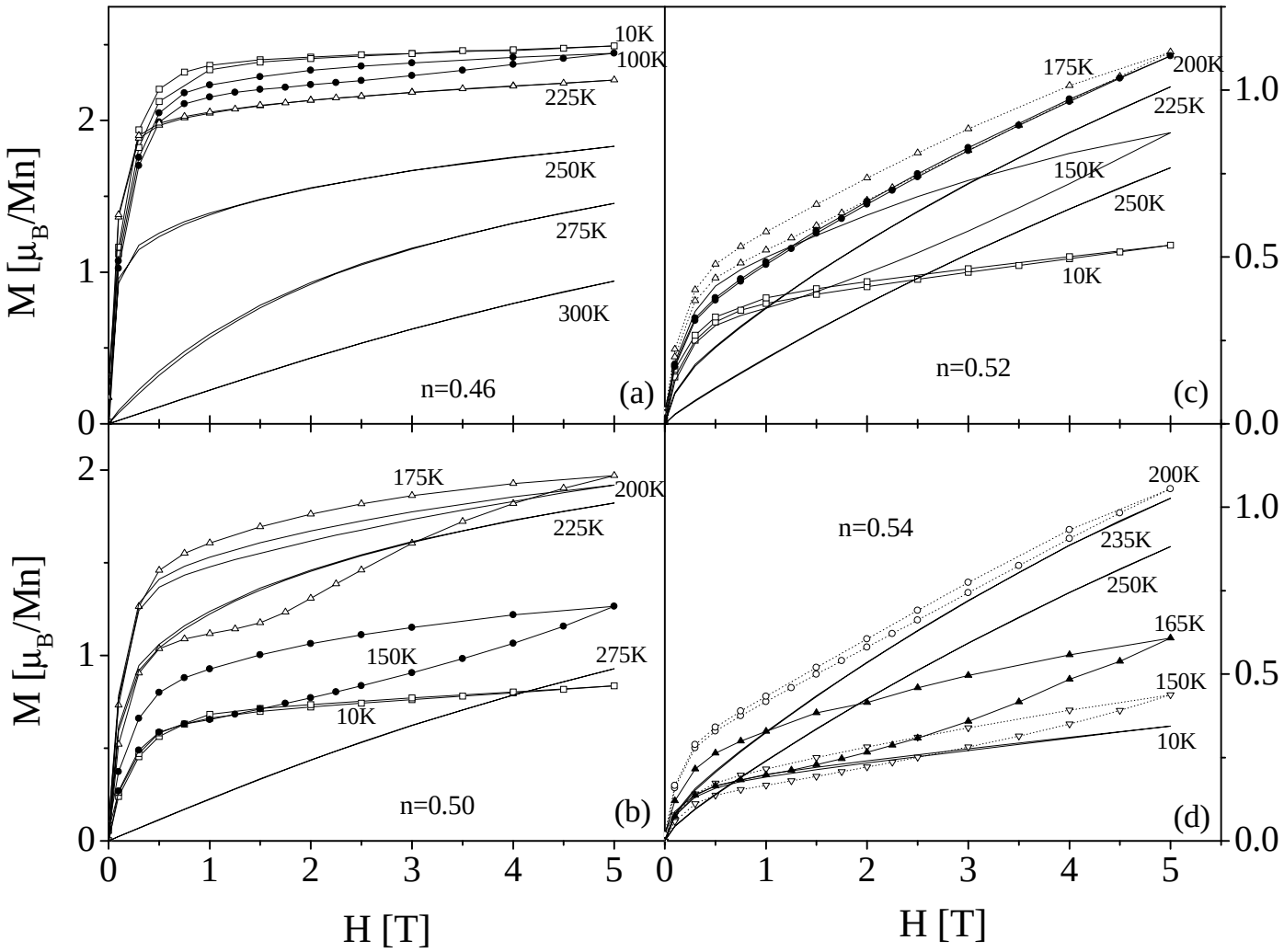
FIG. 11. a) X (at $H = 0T$) as a function of n at $T = 50K$. The dotted line indicates the position of the percolation threshold. b) MR vs n at the same T for several applied magnetic fields, as labeled.

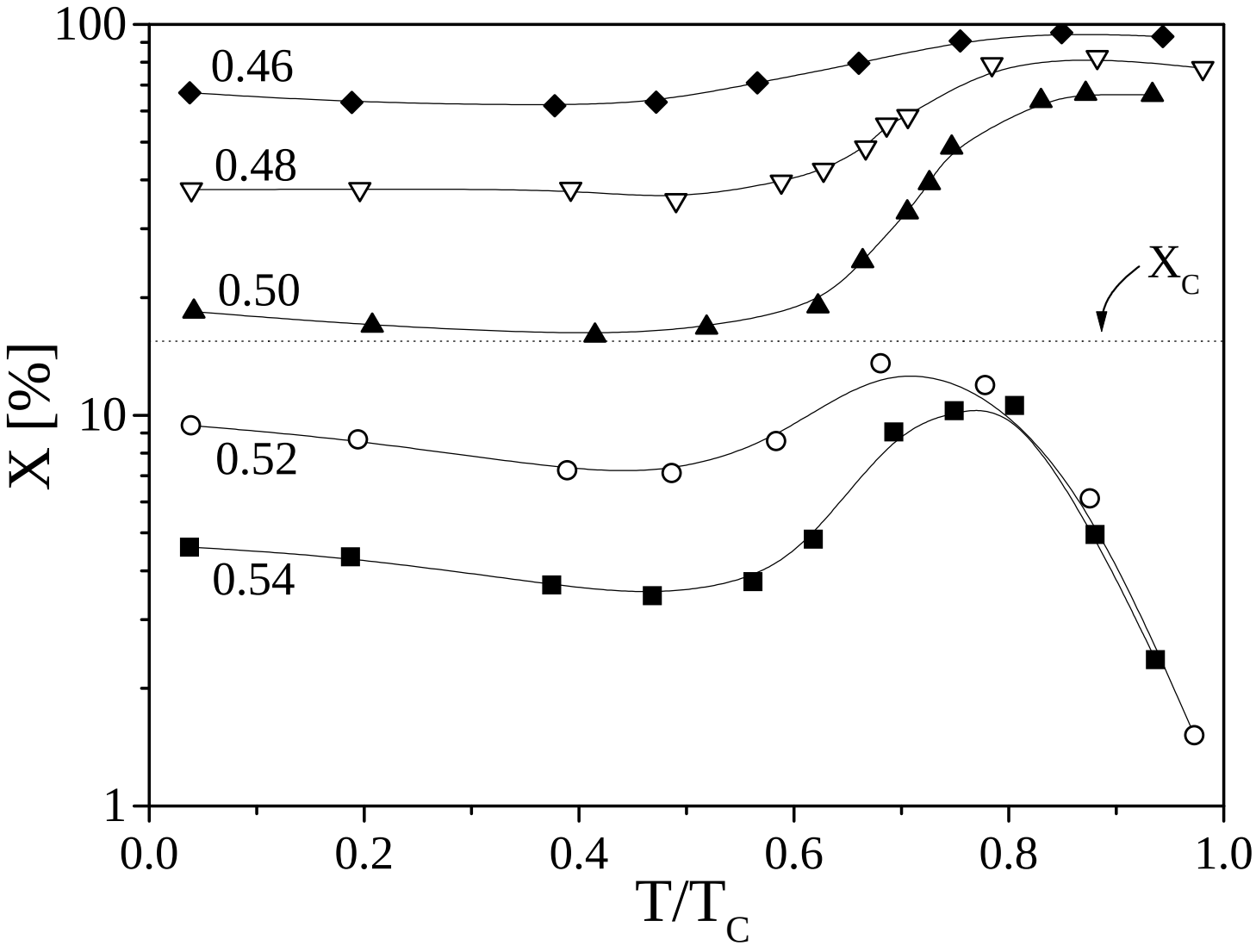
FIG. 12. Phase diagram for the polycrystalline $Pr_{0.5-\delta}Ca_{0.2+\delta}Sr_{0.3}MnO_3$ (hole doping $n = 0.5 + \delta$). Except for $T > T_C$ and between T_C and T_{CO} for $n < 0.50$, the remaining diagram is completely phase separated. Below T_{CO} the CO and FM phases coexist, but the gray region correspond to the percolated samples which follow the indicated percolation law. Below the T_{MI} the FM fraction is frozen and the metallic paths show their intrinsic T dependence. For $n > 0.50$, the T_h indicates the appearance of the additional resonance line in the ESR spectra concomitant with the magnetization increase. Though we call this the F' phase, we cannot distinguish between an additional FM phase and a homogeneous canting of the spins in the AFM volume.

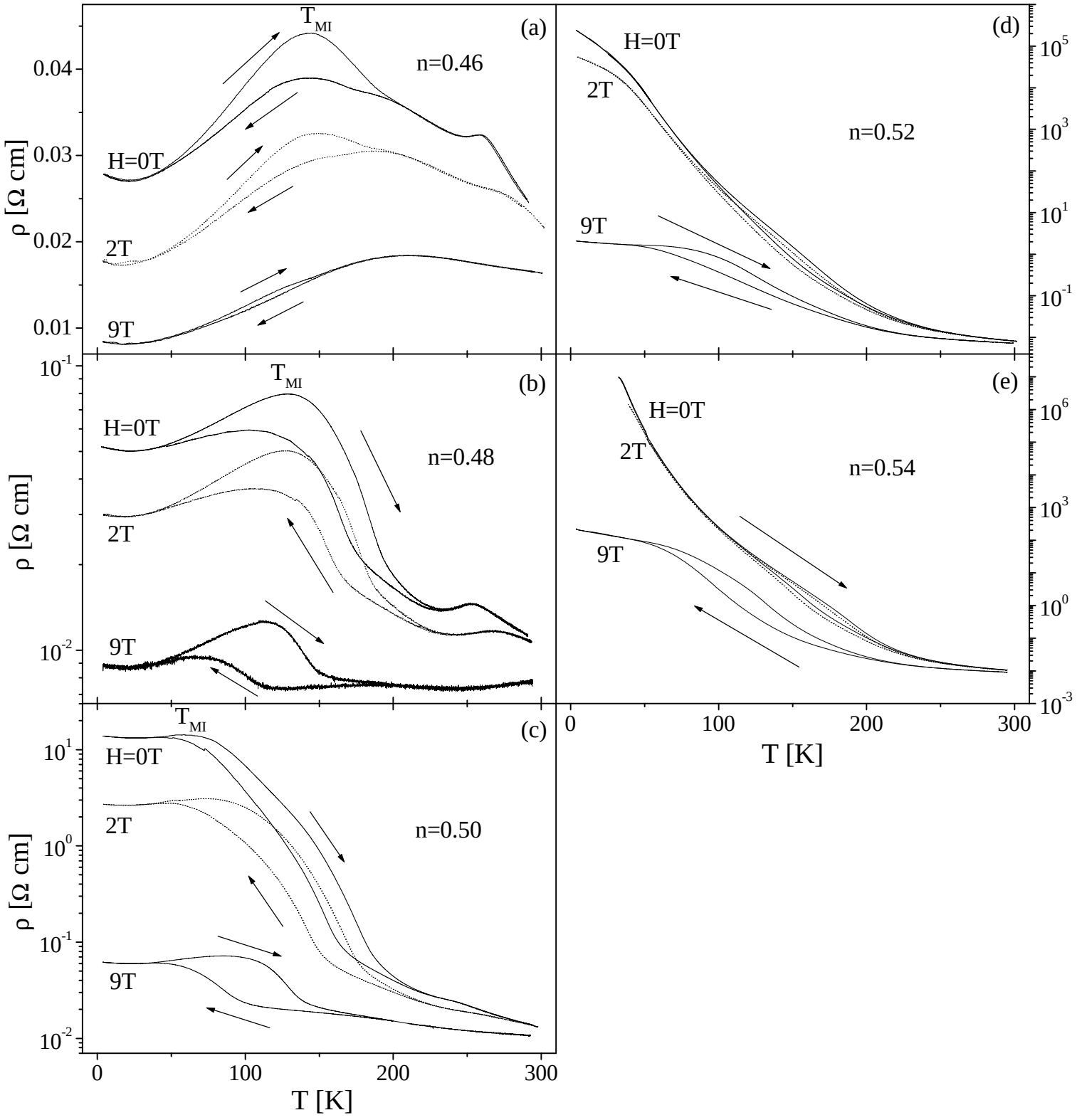

Intensity [arb. units]
1.00
0.75
0.50
0.25
0.00
-0.25
20
40
60
80
100
2θ [degrees]
Pbnm
I4/mcm
difference
Intensity [arb. units]
0.27
0.18
0.09
0.00
46.5
47.0
47.5
48.0
2θ [degrees]
n=0.46
n=0.50
n=0.54
(220) Pbnm
(004) I4/mcm
(004) Pbnm
(220) I4/mcm

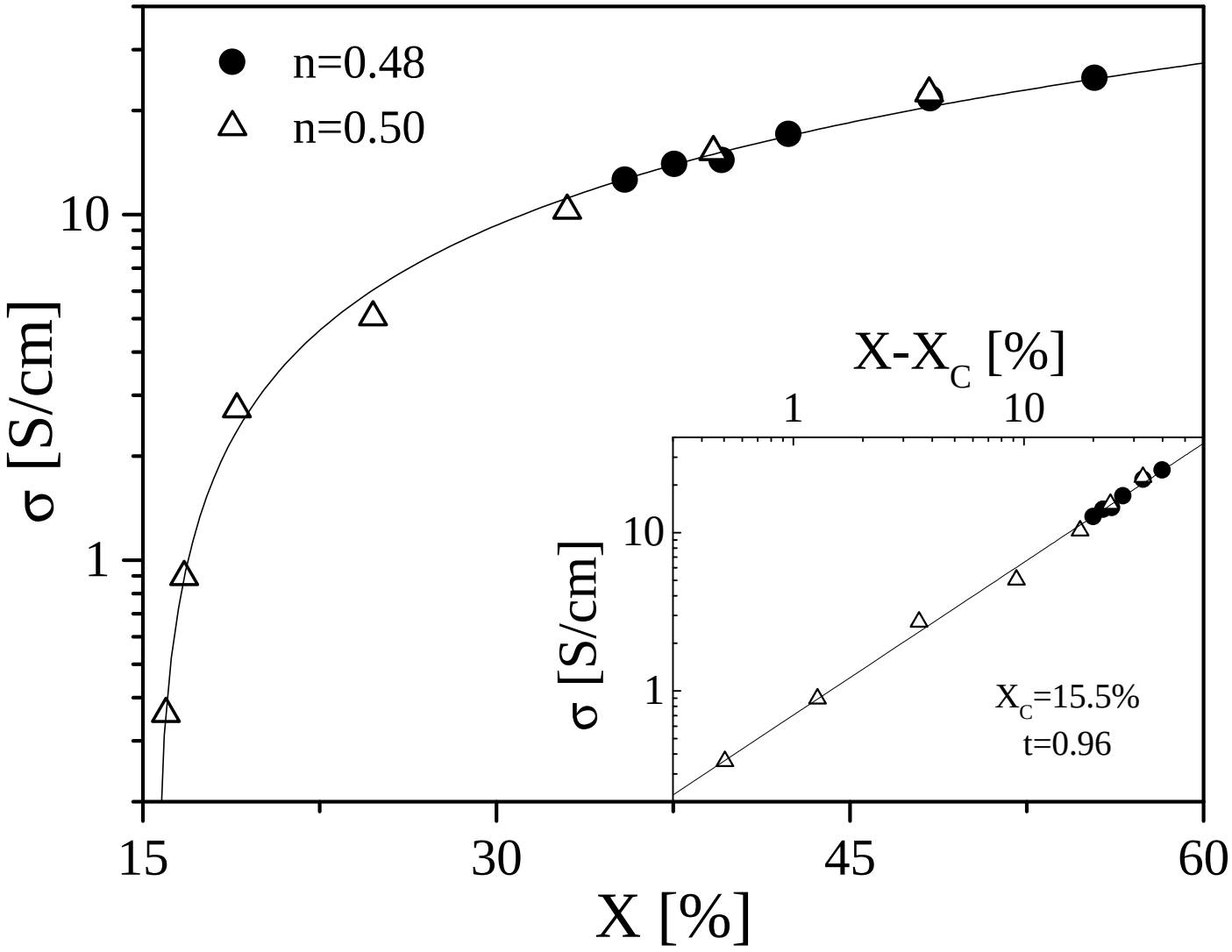

(a)
(b)
(c)
(d)
n=0.46
n=0.48
n=0.50
n=0.52
n=0.54
T_C
T_h
M [μ_B/Mn]
T [K]
0.45
0.30
0.15
0.00
0.18
0.12
0.06
0.042
0.028
0.014
0.033
0.022
0.011
0.000
0
100
200
300

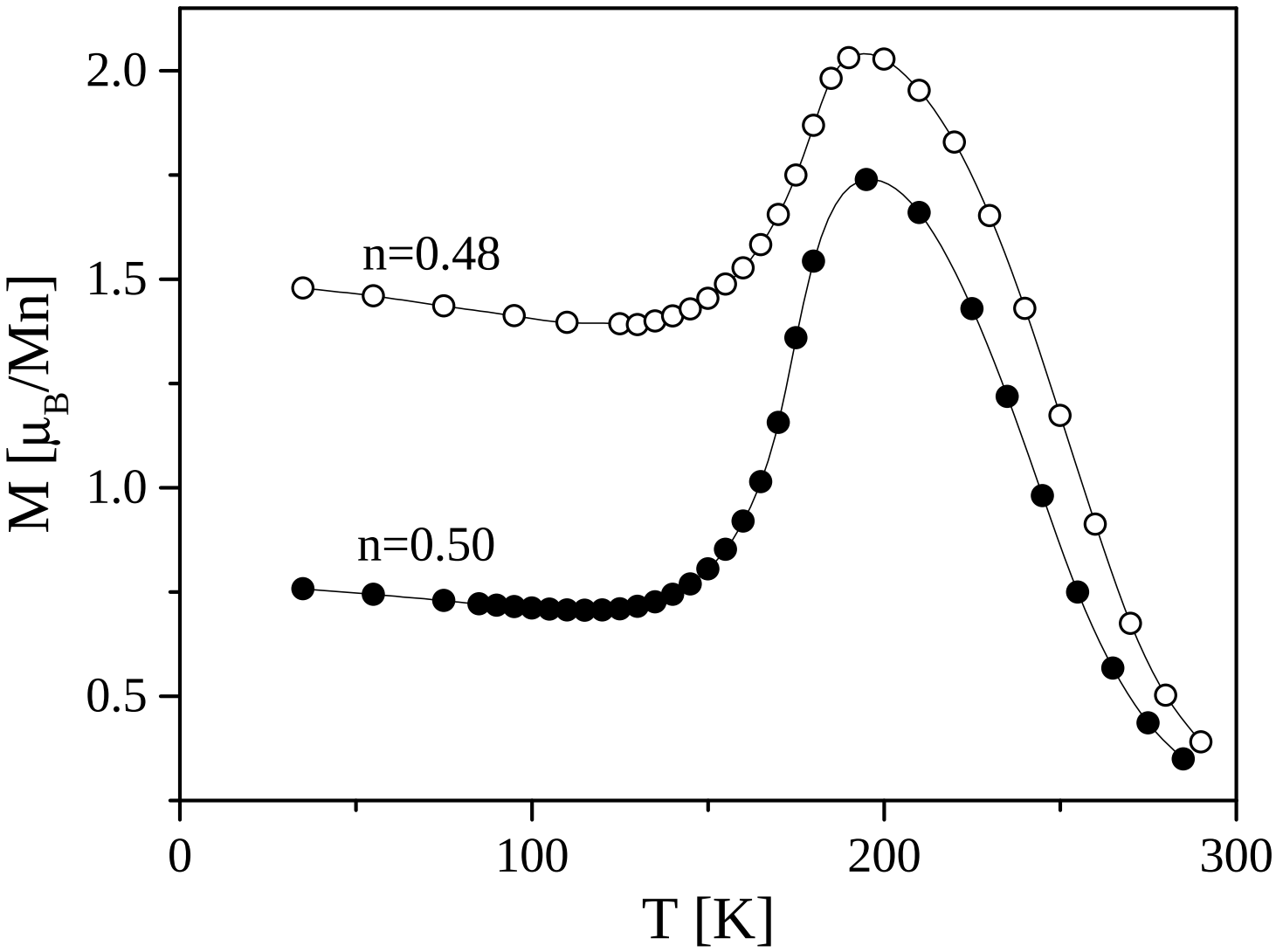

(a)
100 K
0.46
0.48
0.50
0.52
0.54
*
*
(c)
207 K
0.46
0.48
0.50
0.52
0.54
g=2.00
(b)
150 K
0.46
0.48
0.50
0.52
0.54
(d)
270 K
0.46
0.48
0.50
0.52
0.54
g=2.00
0.0
0.5
1.0
1.5
2.0
H [T]
0.0
0.5
1.0
1.5
2.0
H [T]

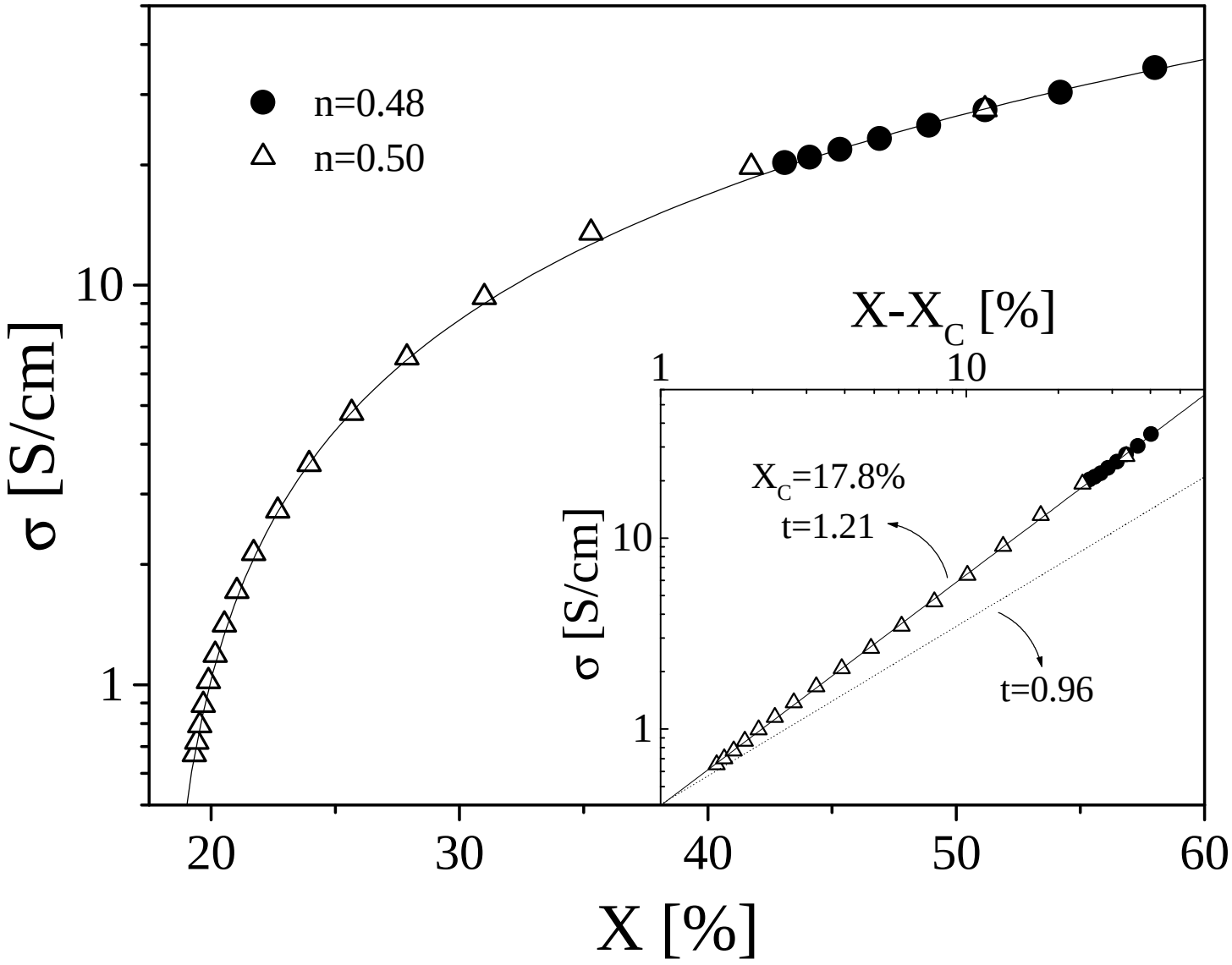

M [μB/Mn]
H [T]
10K
100K
225K
250K
275K
300K
n=0.46
(a)
175K
200K
225K
150K
250K
10K
n=0.52
(c)
175K
200K
225K
150K
275K
10K
n=0.50
(b)
200K
n=0.54
235K
250K
165K
150K
10K
(d)

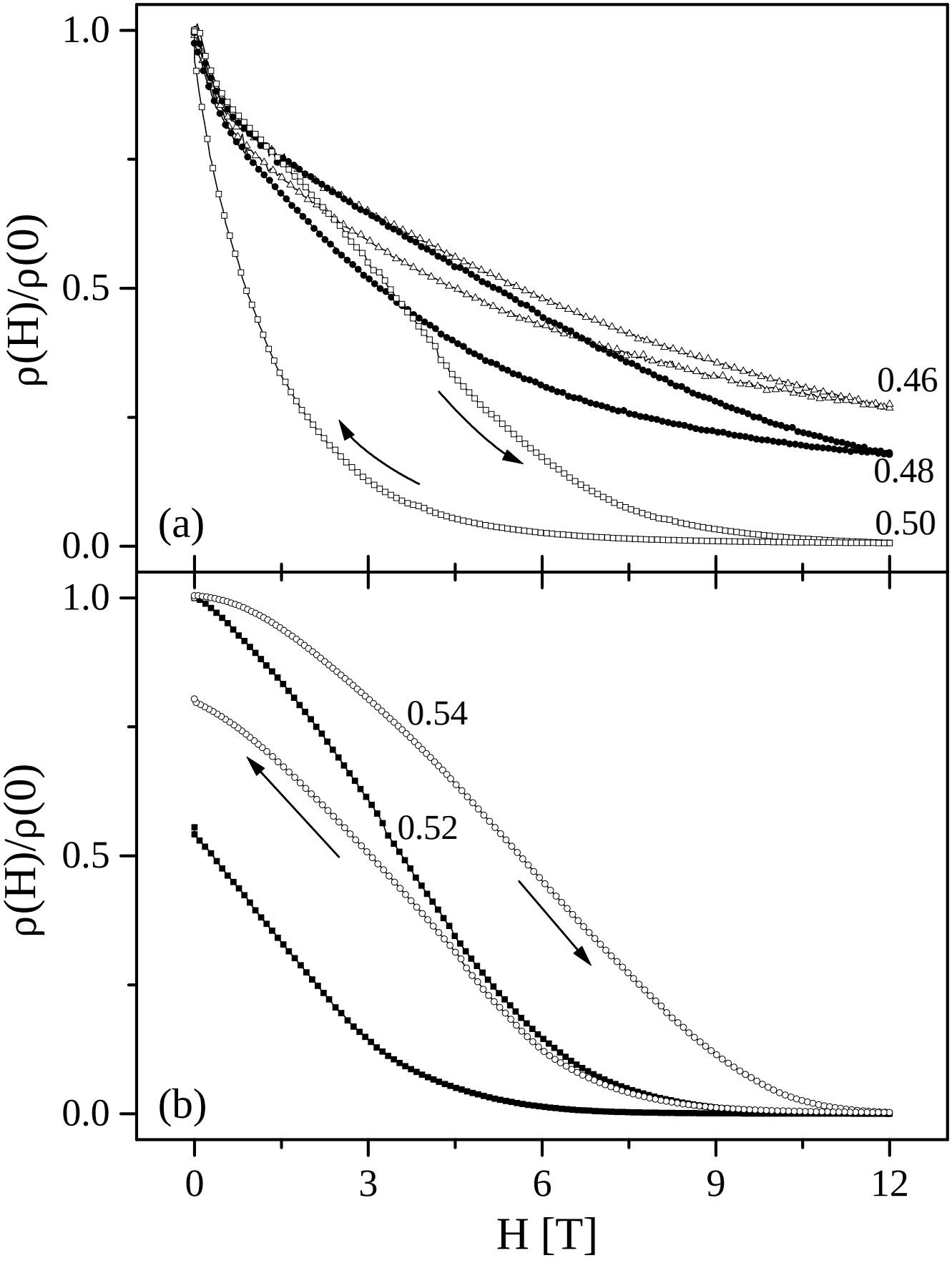

100
10
1
X [%]
0.0
0.2
0.4
0.6
0.8
1.0
T/T_C
0.46
0.48
0.50
0.52
0.54
X_C

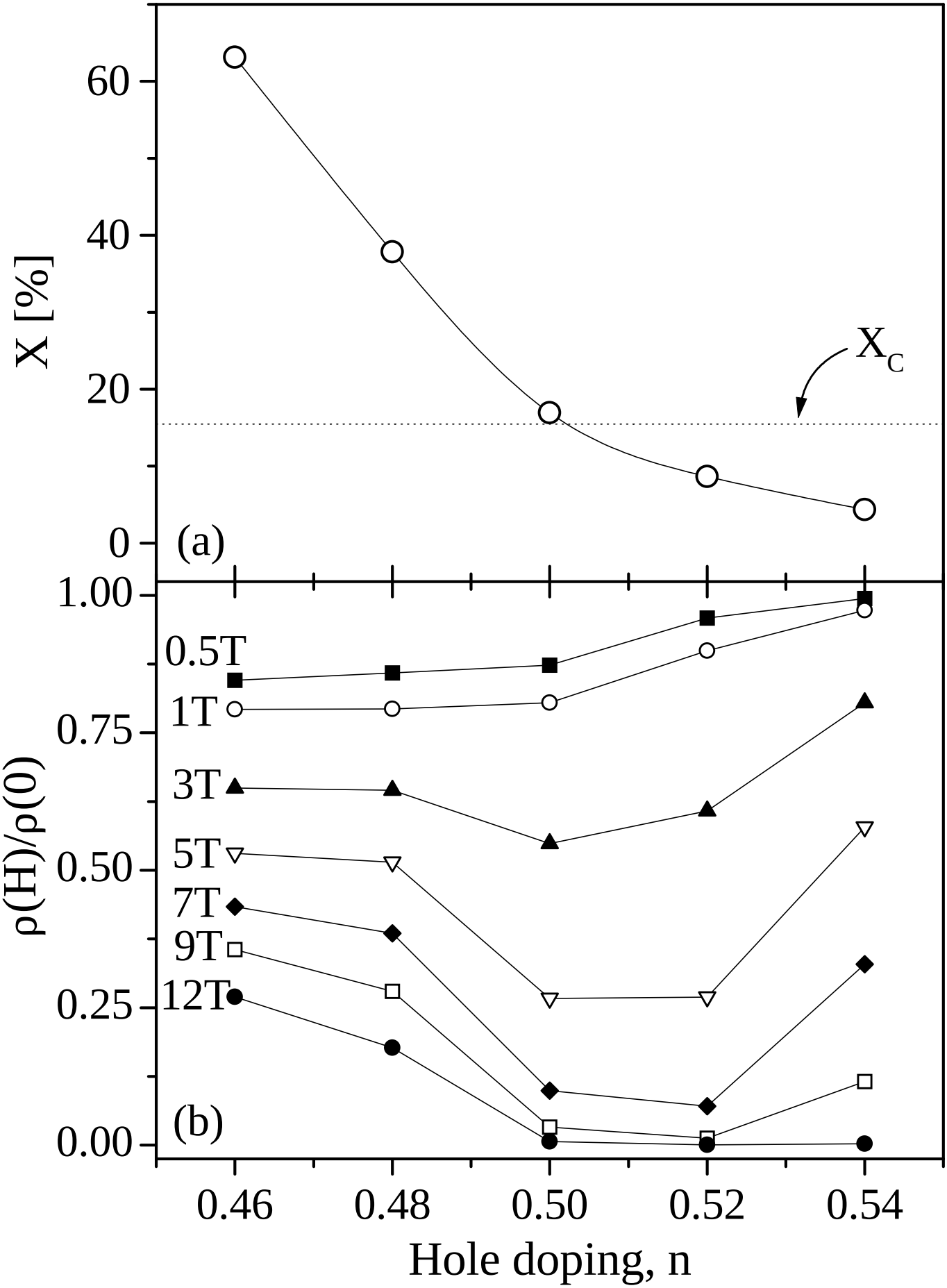

(a)
n=0.46
H=0T
2T
9T
T_{MI}
ρ [Ω cm]
0.04
0.03
0.02
0.01
(b)
n=0.48
H=0T
2T
9T
T_{MI}
10^{-1}
10^{-2}
(c)
n=0.50
H=0T
2T
9T
T_{MI}
10^{1}
10^{0}
10^{-1}
10^{-2}
0
100
200
300
T [K]
(d)
n=0.52
H=0T
2T
9T
10^{5}
10^{3}
10^{1}
10^{-1}
(e)
n=0.54
H=0T
2T
9T
10^{6}
10^{3}
10^{0}
10^{-3}

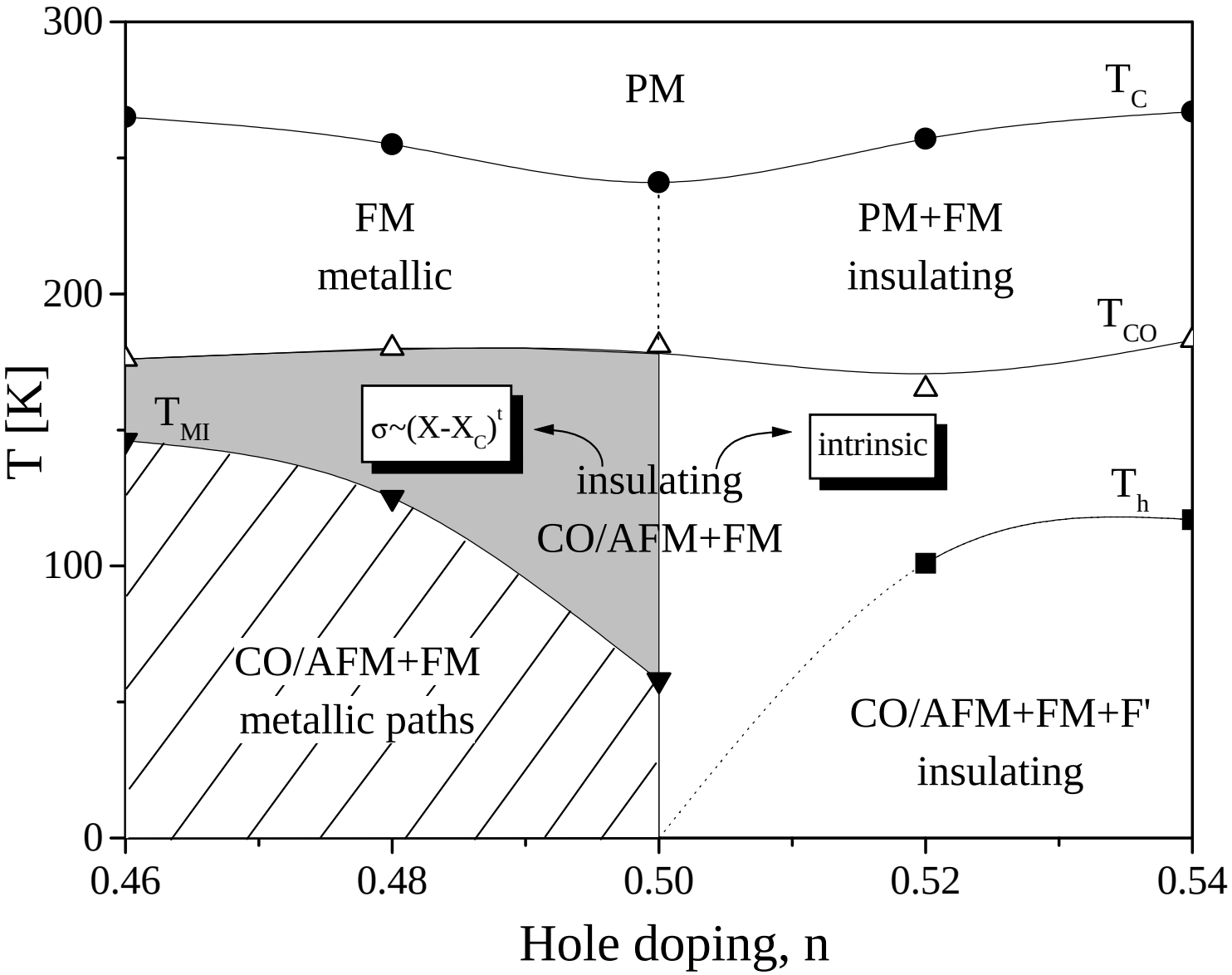

n=0.48
n=0.50
σ [S/cm]
10
1
15
30
45
60
X [%]
X-X_C [%]
1
10
σ [S/cm]
10
1
X_C=15.5%
t=0.96


2.0
1.5
1.0
0.5
M [μB/Mn]
n=0.48
n=0.50
0
100
200
300
T [K]


n=0.48
n=0.50
σ [S/cm]
10
1
20
30
40
50
60
X [%]
X-X_C [%]
1
10
σ [S/cm]
10
1
X_C=17.8%
t=1.21
t=0.96


1.0
0.5
0.0
ρ(H)/ρ(0)
0.46
0.48
0.50
(a)
1.0
0.5
0.0
ρ(H)/ρ(0)
0.54
0.52
(b)
0
3
6
9
12
H [T]


60
40
20
0
X [%]
X_C
(a)
1.00
0.75
0.50
0.25
0.00
ρ(H)/ρ(0)
0.5T
1T
3T
5T
7T
9T
12T
(b)
0.46
0.48
0.50
0.52
0.54
Hole doping, n


300
200
100
0
T [K]
PM
T_C
FM
metallic
PM+FM
insulating
T_CO
T_MI
σ~(X-X_C)^t
insulating
CO/AFM+FM
intrinsic
T_h
CO/AFM+FM
metallic paths
CO/AFM+FM+F'
insulating
0.46
0.48
0.50
0.52
0.54
Hole doping, n